PROCEEDINGS OF SCIENCE

Strangeness photoproduction at the BGO-OD experiment

T.C. Jude[*1], **S. Alef**[1], **P. Bauer**[1], **D. Bayadilov**[2], **R. Beck**[2], **J. Bieling**[1], **A. Bella**[1], **S. Boese**[2], **A. Braghieri**[3], **K. Brinkmann**[4], **D. Burdeynyi**[5], **P. Cole**[1], **R. Di Salvo**[7], **D. Elsner**[1], **A. Fantini**[7,9], **O. Freyermuth**[1], **S. Friedrich**[4], **F. Frommberger**[1], **G. Gervino**[8,9], **F. Ghio**[10,11], **A. Gridnev**[12], **E. Gutz**[4], **D. Hammann**[1], **J. Hannappel**[1], **W. Hillert**[1], **R. Jahn**[2], **R. Joosten**[2], **F. Klein**[1], **K. Kohl**[1], **B. Krusche**[14], **A.M. Lapik**[13], **P. Levi Sandri**[15], **V.P. Lisin**[13], **I. V. Lopatin**[12], **G. Mandaglio**[5,6], **F. Messi**[1], **R. Messi**[7,9], **V. Metag**[4], **D. Moricciani**[7], **A.N. Mushkarenkov**[13], **M. Nanova**[4], **V.G. Nedorezov**[13], **D. Novinskiy**[12], **P. Pedroni**[3], **A.S. Polonski**[13], **B. Reitz**[1], **M. Romaniuk**[8], **G. Scheluchin**[1], **H. Schmieden**[1], **A. Stugelev**[12], **V. Sumachev**[12], **V. Tarakanov**[12], **V. Vegna**[1], **D. Walther**[2], **H. Zaunick**[2,4] **T. Zimmermann**[1]

[1] *Physikalisches Institut, Universität Bonn, Germany,*[2] *Helmholtz-Institut für Strahlen- und Kernphysik, Universität Bonn, Germany,*[3] *INFN sezione di Pavia, Via Agostino Bassi, Pavia, Italy,*[4] *II. Physikalisches Institut, Universität Gießen, Germany,*[5] *INFN sezione Catania, Italy,*[6] *Università degli Studi di Messina, Italy,*[7] *INFN Roma Tor Vergata, Italy,*[8] *INFN sezione di Torino, Italy,*[9] *Dipartimento di Fisica, Università di Torino, Italy,*[10] *INFN sezione di Roma, Italy,*[11] *Istituto Superiore di Sanità, Roma, Italy,*[12] *Petersburg Nuclear Physics Institute, Gatchina, Russid,*[13] *Russian Academy of Sciences Institute for Nuclear Research, Moscow, Russid,*[14] *Institut für Physik, Universität Basel, Switzerland,*[15] *INFN - LNF, Frascati, Italy*

E-mail: jude@physik.uni-bonn.de

The BGO-OD experiment at the ELSA accelerator facility uses an energy tagged bremstrahlung photon beam to investigate the excitation spectrum of the nucleon. The setup consists of a highly segmented BGO calorimeter surrounding the target, with a particle tracking magnetic spectrometer at forward angles. BGO-OD is ideal for investigating the photoproduction of hadrons of non-zero strangeness. The high momentum resolution at forward angles covers a kinematic region where t-channel exchange mechanisms play a dominant role. Access to this low momentum transfer region also allows the investigation of degrees of freedom not derived from constituent quark models, for example, the role of (vector) meson - baryon interactions and dynamically generated states in photoproduction reactions. Data taking for the first part of an extensive physics programme is complete and preliminary results and ongoing analysis are presented.

XVII International Conference on Hadron Spectroscopy and Structure - Hadron2017
25-29 September, 2017
University of Salamanca, Salamanca, Spain

[*]Speaker.

PoS(Hadron2017)054

1. Introduction

The excitation spectrum of the nucleon constrains our understanding of the degrees of freedom afforded to the constituents and their interactions in non-peturbative QCD. Constituent quark models (CQM) where "dressed" quarks are bound in a mutually generated potential describe this spectrum with limited success. The pattern of the mass and parity of the Roper resonance ($N(1440)1/2^+$) and the $N(1535)1/2^-$, the $\Lambda(1405)$ - $N^*(1535)$ mass ordering, and the mass between the $\Lambda(1405)$ and its spin-orbit partner, $\Lambda(1520)$, are all difficult to reconcile with a CQM. Models explicitly including meson-baryon interactions as further degrees of freedom have had success in describing such states (see for example refs. [1, 2, 3, 4, 5]). The $\Lambda(1405)$ for example, appears to be dynamically generated from meson-baryon interactions to some extent [6], which is also supported by recent LQCD calculations [7]. Models including vector meson-baryon interactions have predicted further dynamically generated states, for example states at 2 GeV with $J^P = 1/2^-$ and $3/2^-$ [8, 9, 10], which may have been observed in $K^0\Sigma^+$ photoproduction [11, 12] at the K^*Y thresholds. Equivalently, models have also described the pentaquark states, $P_c(4450)^+$ and $P_c(4380)^+$ [13] as dynamically generated through rescattering effects just below the $\bar{D}^*Y_c$ thresholds [14]. Threshold dynamics appear to play a crucial role in mass generation; due to the proximity of the chiral symmetry breaking scale to the nucleon mass, it is possible that light mesons may interact as elementary objects, giving rise to molecular systems and meson rescattering effects near thresholds [15, 16].

The BGO-OD experiment [17, 18, 19] has an extensive range of strangeness photoproduction proposals, with the first large dataset taken earlier this year[1]. The extremely forward charged particle acceptance, complemented by neutral particle reconstruction over a central region, allows the study of low momentum exchange processes and complicated mixed charge final states. This combination enables the study for the first time of reaction mechanisms which may manifest from molecular or exotic structure in the strange quark sector.

2. The BGO-OD experiment

BGO-OD is a fixed target experiment at the ELSA electron accelerator facility [20]. An electron beam up to 3.2 GeV is incident upon a thin metal radiator to produce energy tagged bremsstrahlung photons, with linearly and circularly polarised beams both available.

BGO-OD (fig. 1 (top left)) is composed of two distinct parts: A central calorimeter region ($\theta = 25 - 155^0$) and a forward spectrometer ($\theta < 12^0$). The acceptance hole between these is covered by a plastic scintillating detector (SciRi).

A liquid hydrogen, deuterium or nuclear target is at the centre of the central region. An MWPC surrounds the target for charged particle track reconstruction and accurate determination of the reaction vertex. Outside of this is a segmented cylinder of plastic scintillator material for charged particle identification via $\Delta E - E$. Surrounding this is the BGO ball; a segmented calorimeter of 480 bismuth germanate crystals. The BGO ball is ideal for the reconstruction of photon four-momenta via clustering algorithms to characterise the electromagnetic showers in the crystals. The separate

[1] There are additional studies into η' threshold production and non-strange vector meson photoproduction.

time readout per crystal, with a resolution of approximately 3 ns, enables clean identification of neutral meson decays (fig. 1 (top middle and right)).

The forward spectrometer uses two scintillating fibre detectors (SciFi2 and MOMO) to track charged particles from the reaction or decay vertex. Particles then proceed through the open dipole magnet, operating at a maximum field strength of 0.45 T ($\int Bdl \approx 0.45$ Tm). Downstream are eight double layered drift chambers to track particle trajectories after curvature in the magnetic field. Tracking algorithms reconstruct the trajectory and particle momentum, p, with a resolution of approximately $0.04p$. Time Of Flight walls downstream from the drift chambers enable particle identification via the combination of momentum and β (fig. 1, bottom).

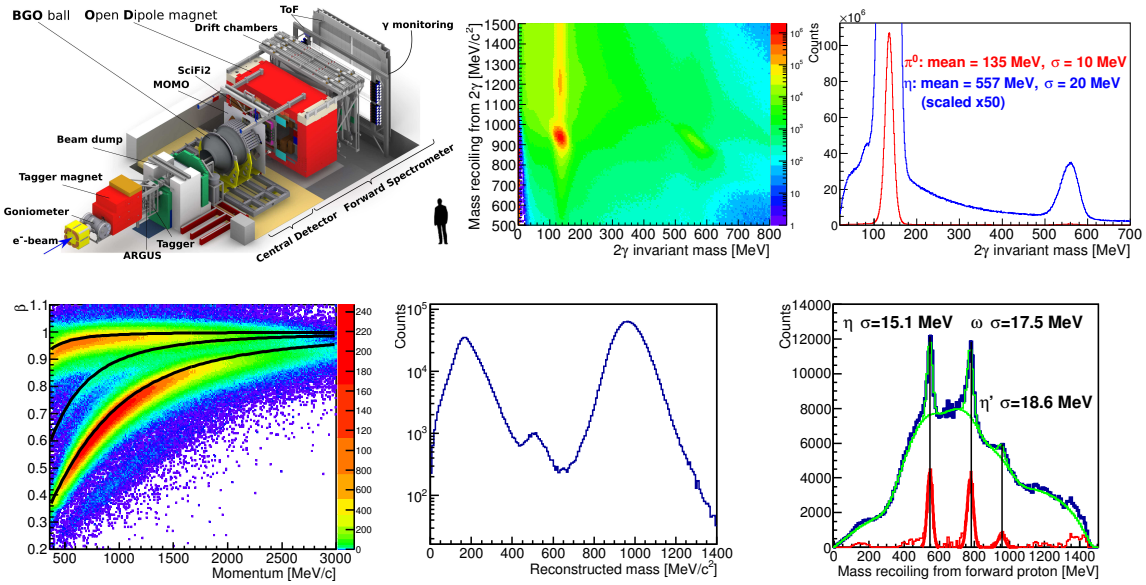

Figure 1: The BGO-OD experiment (Top left). Top centre: The mass recoiling from two photons in the final state versus the invariant mass of the photons. Peaks consistent with $\pi^0 p$ and ηp are visible. Top right: Two photon invariant mass after selecting recoiling proton mass. Bottom left: Charged particle identification in the forward spectrometer. Black lines indicate the expected loci for π^+, K^+ and protons. Bottom centre: Particle mass reconstructed from β and momentum. Bottom right: The mass recoiling from forward protons. Background and peaks corresponding to η, ω and η' masses labelled inset.

3. Strangeness photoproduction: Preliminary results and current analysis

A prerequisite for the study of higher mass hyperons at low t is forward differential cross sections for $K^+\Lambda$ and $K^+\Sigma^0$. This is also a crucial kinematic region missing from the world data set, where the dearth of data prevents the constraining of isobar models [21] and the description of dominating t-channel mechanisms. The forward cross section is also vital to model hypernuclei electroproduction (see for example ref. [22]).

Differential cross sections for $K^+\Lambda$ and $K^+\Sigma^0$ for $\cos\theta^{K^+}_{cm} > 0.9$, binned into 0.02 $\cos\theta^{K^+}_{cm}$ intervals are anticipated soon. The recoil polarisation observable, P_Λ is also being extracted via the asymmetry of the self-analysing $\Lambda \to \pi^0 n$ decay. Fig. 2 shows the mass recoiling from forward K^+,

with peaks at the Λ and Σ^0 masses. The dominant background is uncorrelated e^+e^- pairs from the beam which are in random coincidence with other hardware triggers. Selecting negatively charged particles allows this background to be described and subtracted from the signal. At higher beam energies, background from misidentified π^+ is subtracted by using simulated data.

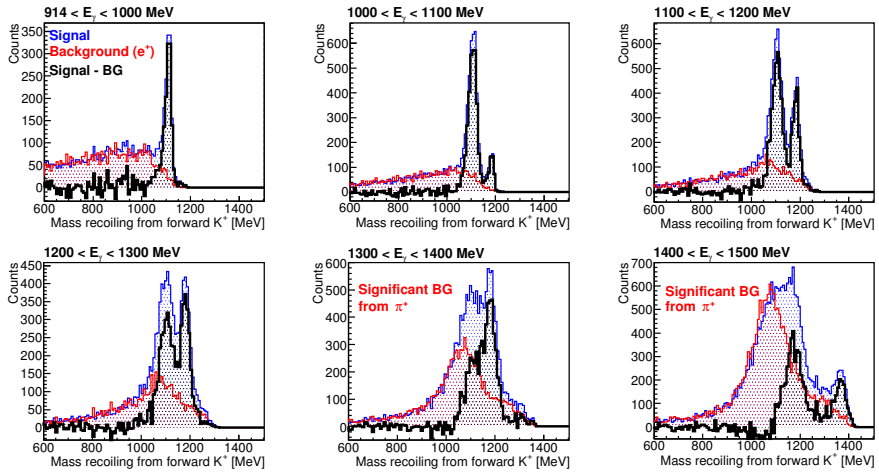

Figure 2: Mass recoiling from forward K^+ for different beam energy, E_γ intervals (inset). Blue: signal, red: background, black: Signal - background.

Fig. 3 shows the mass recoiling from K^+ for all E_γ. A hyperon mass range up to 2 GeV in this low t region can be accessed for the first time, covering a range of poorly described or known Σ^* states (see the review in ref. [23] for example). Additional mesons can be identified in the BGO calorimeter for a separation of K^+Y^* states, shown in fig. 3 (bottom left). Fig. 3 (bottom right) is a preliminary $\Lambda(1405) \rightarrow \pi^0\Sigma^0$ lineshape for $\cos\theta^{K^+}_{cm} > 0.9$, after the removal of the overlapping $\Sigma(1385)$.

Fig. 4 shows the reconstruction of $K^+\Sigma^0$ via the identification of $K^+\gamma p\pi^-$ over a broad angular range. Selected events were subjected to a kinematic fit and the application of neural network techniques to remove background. The preliminary differential cross section demonstrates good agreement with previous publications and nearly 4π angular acceptance. This analysis is a control for reconstructing complicated mixed charge final states that is vital for higher mass hyperons.

An equivalent analysis for identifying $K^+\pi^0 p\pi^-$ (one additional photon) was used to determine the $\Lambda(1405) \rightarrow \pi^0\Sigma^0$ line shape shown in fig. 5 (left) over a broad angular acceptance. Fig. 5 (right) is the first analysis for $\Lambda(1405) \rightarrow \pi^+\Sigma^-$ at low momentum transfer.

The model of Oset and Ramos [10] which described the cusp-like structure in $K^0_S\Sigma^+$ photoproduction [11] as a destructive interference between vector meson-baryon dynamically generated states, predicts a peak from constructive interference for $\gamma n \rightarrow K^0_S\Sigma^0$. The study of both channels is vital to elucidate the role of K^* exchange and the relevant degrees of freedom in the reaction mechanism. K^0_S can be identified via both charged and neutral pion decays at BGO-OD, shown in fig. 6 (left and centre) using a liquid hydrogen target. Fig. 6 (right) shows analysis from a commissioning beam time using a deuterium target, where the $K^0_S\Sigma^0$ channel was identified via the neutral kaon decay. Data taking with a deuterium target is anticipated early next year.

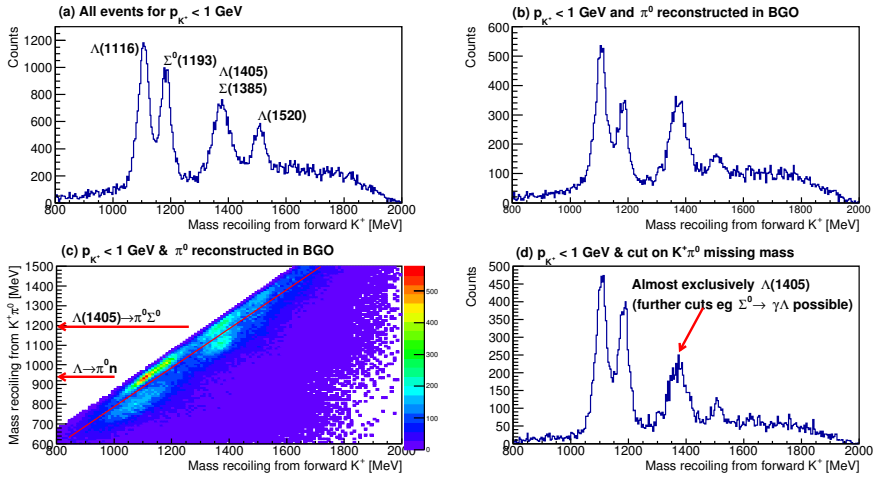

Figure 3: Mass recoiling from K^+ identified in the forward spectrometer. (a) All events for K^+ with a momentum below 1 GeV/c. Peaks corresponding to hyperon masses are labelled inset. (b) Equivalent histogram with an additional π^0 identified in the BGO. (c) Equivalent histogram with a y-axis of the mass recoiling from the $K^+\pi^0$ system. The red line separates $K^+\Lambda(1405)$ and $K^+\Sigma(1385)$ events. (d) After rejecting $K^+\Sigma(1385)$ events. A preliminary, non-acceptance corrected $\Lambda(1405) \to \pi^0\Sigma^0$ lineshape is shown above background.

References

[1] R.H. Dalitz, T.C. Wong and G. Rajasekaran, Phys. Rev. **153**, 1617 (1967)

[2] P.B. Siegel and W. Weise, Phys. Rev. **C 38**, 2221 (1988)

[3] N. Kaiser, T. Waas and W. Weise, Nucl. Phys. **A 612**, 297 (1997)

[4] C. Garcia-Recio, M.F.M. Lutz, and J. Nieves, Phys. Lett. **B 582**, 49 (2004)

[5] M.F.M. Lutz and E.E. Kolomeitsev, Phys. Lett. **B 585**, 243 (2004)

[6] J.C. Nacher, E. Oset, H. Toki, A. Ramos, U.G. Meissner, Nucl. Phys. **A 725**, 181 (2003)

[7] J.M.M Hall *et al.*, Phys. Rev. Lett. **114**, 132002 (2015)

[8] P. Gonzalez, E. Oset and J. Vijande, Phys. Rev. **C 79**, 025209 (2009)

[9] S. Sarkar *et al.*, Eur. Phys. J. **A 44**, 431 (2010)

[10] E. Oset and A. Ramos, Eur. Phys. J. **A 44**, 445 (2010)

[11] R. Ewald *et al.*, Phys. Lett. **B 713**, 180 (2012)

[12] R. Ewald *et al.*, Phys. Lett. **B 738**, 268 (2014)

[13] R. Aaij *et al.*, Phys. Rev. Lett **115**, 072001 (2015)

[14] Jia-Jun Wu, R. Molina, E. Oset, and B.S. Zou, Phys. Rev. Lett. **105**, 232001 (2010)

[15] A. Manohar and H. Georgi, Nucl. Phys. **B 234**, 189 (1984)

[16] L.Ya. Glozman and D.O. Riska, Physics Reports **268**, 263 (1996)

[17] B. Bantes *et al.*, Int. J. Mod. Phys: Conf. Ser. **26**, 1460093 (2014)

[18] H. Schmieden, Int. J. Mod. Phys. **E 19**, 1043 (2010)

[19] H. Schmieden, Ch. Phys. **C 33**, 1146 (2009)

[20] W. Hillert, Eur. Phys. J. **A 28**, s01, 139 (2006)

[21] Bydzovsky and D. Skoupil, arXiv:1211.2684v1 (2012) Proceedings of SNP12.

[22] R. Shyam, K. Tsushima, A.W. Thomas, Phys. Lett. **676**, 51 (2009)

[23] C. Patrignani *et* al. (Particle Data Group), Chin. Phys. **C 40**, 100001 (2016)

[24] K.H. Glander *et al.*, Eur. Phys. J. **A 19**, 251 (2004)

[25] M. Sumihama *et al.*, Phys. Rev. **C 73**, 035214 (2006)

[26] B. Dey, C.A. Meyer, M. Bellis, M.E. McCracken, M. Williams *et al.*, Phys. Rev. **C 82**, 025202 (2010)

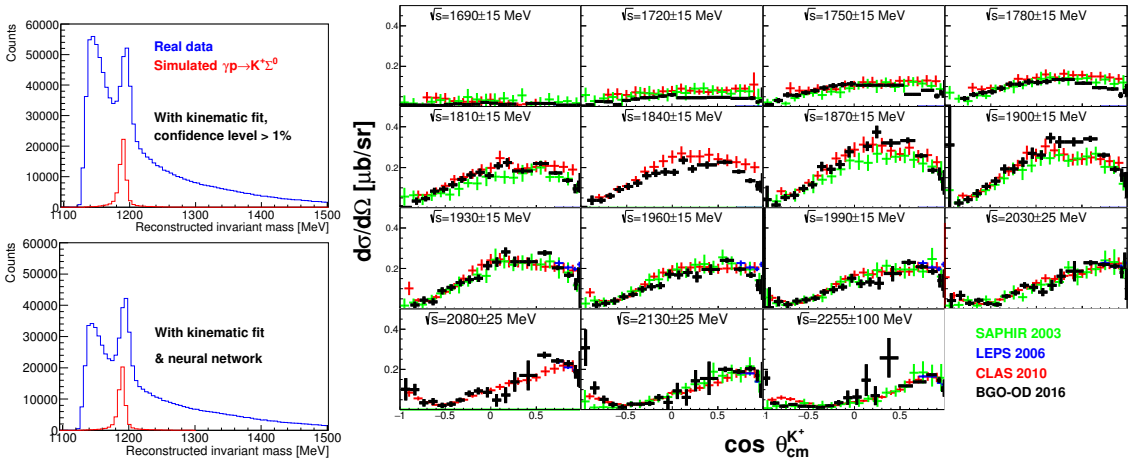

Figure 4: Left: The identification of $\gamma p \to K^+\Sigma^0$ via the detection of K^+, γ, proton and π^- for real (blue) and simulated data (red). Right: Preliminary differential cross sections (black), compared to previous SAPHIR [24], LEPS [25] and CLAS [26] data. Analysis by G. Scheluchin.

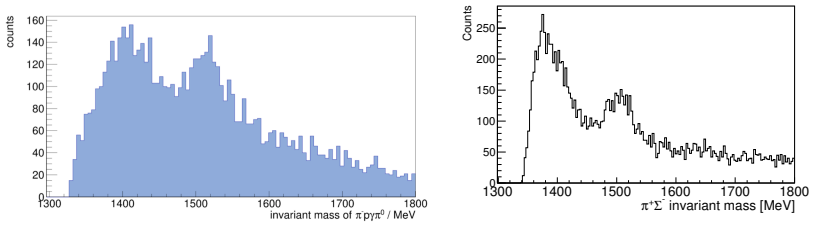

Figure 5: Preliminary, non-acceptance corrected and no background subtracted $\Lambda(1405)$ lineshape for $\Lambda(1405) \to \pi^0\Sigma^0$ over a broad kinematic range (left), and $\Lambda(1405) \to \pi^+\Sigma^-$ when the K^+ is identified in the forward spectrometer (right). Analysis by G. Scheluchin.

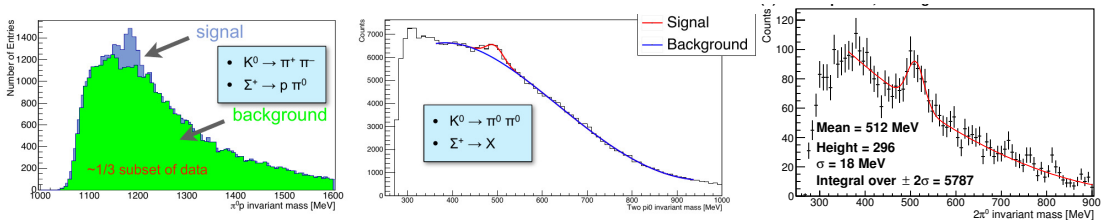

Figure 6: Top: Preliminary analysis of $\gamma p \to K^0_S\Sigma^+$, prior to kinematic fits. Left: Identification via $\gamma p \to K^0_S(\to \pi^+\pi^-)\Sigma^+$ (blue), with background described using simulated data in green. Centre: Identification via $\gamma p \to K^0_S(\to 2\pi^0)\Sigma^+$. A 3rd order polynomial and Gaussian are fitted to background and signal respectively. Analysis by B.E- Reitz and S. Alef. Right: $\gamma n \to K^0_S(\to 2\pi^0)\Sigma^0$ reconstruction using commissioning deuterium target data. A recoiling mass consistent with a π^- is selected from the $2\pi^0 p$ system, where the proton is detected in the forward spectrometer. A second order polynomial and Gaussian function describe the background and K^0_S invariant mass signal respectively (parameters inset).